

PREPARED FOR SUBMISSION TO JHEP

Top and bottom quark forward-backward asymmetries at next-to-next-to-leading order QCD in (un)polarized electron positron collisions

Werner Bernreuther,^a Long Chen,^b Peng-Cheng Lu,^b Zong-Guo Si^b

^a*Institut für Theoretische Teilchenphysik und Kosmologie,
RWTH Aachen University, 52056 Aachen, Germany*

^b*School of Physics, Shandong University, Jinan, Shandong 250100, China*

E-mail: breuther@physik.rwth-aachen.de, longchen@sdu.edu.cn,
pclu@sdu.edu.cn, zgzi@sdu.edu.cn

ABSTRACT: We consider, at order α_s^2 in the QCD coupling, top-quark pair production in the continuum at various center-of-mass energies and b -quark pair production at the Z resonance by (un)polarized electron and positron beams. For top quarks we compute the forward-backward asymmetry with respect to the top-quark direction of flight, the associated polar angle distribution, and we analyze the effect of beam polarization on the QCD corrections to the leading-order asymmetry. We calculate also the polarized forward-backward asymmetry. For b -quark production at the Z peak we explore different definitions of A_{FB} . In particular, we analyze b jets defined by the Durham and the flavor- k_T clustering algorithms. We compute the inclusive b -jet and two-jet asymmetry with respect to the b -jet direction. For the latter asymmetry the QCD corrections to order α_s^2 are small. That predestines it to act as a precision observable.

Contents

1	Introduction	1
2	The forward-backward and polarized forward-backward asymmetry	3
3	Asymmetries for top quarks	6
4	Asymmetries for b-quark pair production at the Z peak	12
5	Conclusions	19

1 Introduction

Among the various high-energy particle accelerator types that are presently discussed for potential future realization, an electron-positron collider has the highest priority. Several proposals for a linear [1–3] and a circular [4, 5] e^+e^- collider have been made. The major motivation for such a machine is to construct a Higgs factory with which the properties of the 125 GeV Higgs boson can be studied with unprecedented precision. Besides, such a machine would allow for new physics searches and precision studies of weak gauge bosons and heavy quarks, in particular top quarks (see, for instance, [6, 7]). Longitudinal polarization of e^- and e^+ beams, which is a prospective option especially for linear colliders, is a further asset in the exploration of the fundamental interactions at high energies.

As far as the physics of top and bottom quarks at a future linear or circular e^+e^- collider is concerned, the measurement of forward-backward asymmetries (A_{FB}) will play a prominent role, in particular for the precision determinations of electroweak parameters. On the theory side, this requires precise predictions, in particular of the higher-order QCD corrections to these asymmetries.

For massive quark-antiquark production in e^+e^- collisions the following Standard Model (SM) radiative corrections to the lowest-order forward-backward asymmetry are known so far. The fully massive next-to-leading order (NLO) electroweak and QCD corrections were determined in [8–12] and in [13–18], respectively. The heavy quark pair production cross section was computed to order α_s^2 and order α_s^3 in [19–22] and [23, 24], respectively, using approximations.¹ The fully differential $t\bar{t}$ cross section at NLO QCD with $t \rightarrow Wb$ decay was investigated in [26] and recently, the NLO QCD corrections to off-shell $t\bar{t}$ production with semi-leptonic top-quarks decays were computed in [27]. The full next-to-next-to-leading order (NNLO), i.e. the order α_s^2 QCD corrections to A_{FB} were computed by [28, 29] for the top quark in $t\bar{t}$ production above the production threshold.

¹The complete electroweak two-loop corrections for typical precision observables at the Z resonance were finalized in [25]; cf. also further references therein.

A considerable effort was made to investigate $t\bar{t}$ production at threshold, presently known at next-to-next-to-next-to-leading (NNNLO) order QCD [30–33]. Recently, the NNNLO QCD correction to $e^+e^- \rightarrow t\bar{t}$ production in the continuum via a virtual photon was obtained in [34] with the powerful auxiliary-mass flow method [35–39]. For $b\bar{b}$ production at the Z peak, the order α_s^2 corrections were calculated for several definitions of the b -quark forward-backward (FB) asymmetry for massless b quarks by [40–43] and for massive quarks in [44], and also in [45] where the optimization based on the principle of maximum conformality [46–48] was taken into account.

In this paper we extend the present theory knowledge of the top- and bottom-quark A_{FB} in several ways. In particular we investigate the effect of beam polarization on these asymmetries. As far as $t\bar{t}$ production in the continuum is concerned we calculate the order α_s^2 QCD corrections to the top-quark A_{FB} with respect to the top-quark direction of flight for a set of longitudinal polarizations of the e^- and e^+ beams and compare with the respective A_{FB} resulting from top-quark production with unpolarized beams. We find a marginal dependence of the QCD corrections on beam polarization. As to $e^+e^- \rightarrow b\bar{b}$ at the Z resonance, we consider also production by polarized beams and compare with results for unpolarized beams. We compute the order α_s^2 QCD corrections to the b -quark A_{FB} for the cases where the forward and backward hemispheres are defined with respect to the b -quark direction of flight and the oriented thrust axis. Moreover, we consider b jets defined by the Durham [49] and flavor- k_T [50] algorithm, use the resulting b -jet axis for defining A_{FB} , and compute the order α_s^2 QCD corrections to an inclusive b -jet asymmetry and to the two-jet asymmetry. The latter A_{FB} was calculated before to order α_s in [15] and for massless b quarks to order α_s^2 in [43]. As in the massless case, the QCD corrections to this asymmetry are small. Thus it may serve as a suitable precision observable.

Our paper is organized as follows. section 2 contains formulas for A_{FB} to order α_s^2 , unexpanded and expanded in the QCD coupling, for the polarized forward-backward asymmetry [51], and a set of beam polarizations that will be used in the following sections. In section 3 we investigate $t\bar{t}$ production to order α_s^2 by polarized and unpolarized beams at c.m. energies 380 GeV, 400 GeV, 500 GeV, and 700 GeV. The forward and backward hemispheres are defined with respect to the top-quark direction of flight and we compute the symmetric (σ_S) and antisymmetric (σ_A) cross sections and A_{FB} to order α_s^2 . We analyze the effect of beam polarization on the QCD corrections to the leading-order FB asymmetry. For the c.m. energy 500 GeV we determine the polar angle distribution of the top quark for (un)polarized beams. In addition we calculate the polarized FB asymmetry for the c.m. energies listed above. In section 4 we consider $b\bar{b}$ production to order α_s^2 at the Z -boson resonance by (un)polarized beams. Here we explore different definitions of the forward and backward hemispheres. First we use the b -quark axis and the oriented thrust axis and determine σ_S , σ_A , and the resulting A_{FB} . Then we turn to b jets defined by i) the Durham and ii) the flavor- k_T clustering algorithm. Related to the respective b -jet direction we compute the inclusive b -jet and two-jet asymmetry. We comment also briefly on the electroweak corrections to the b -quark asymmetries. We conclude in section 5.

2 The forward-backward and polarized forward-backward asymmetry

In this paper we consider the production of top-quark and bottom-quark pairs in (un)polarized e^+e^- collisions,

$$e^-(\mathbf{p}_1) + e^+(\mathbf{p}_2) \rightarrow Q(\mathbf{k}_1) + \bar{Q}(\mathbf{k}_2) + X, \quad Q = t, b, \quad (2.1)$$

to lowest order in the electroweak couplings and to second order in the QCD coupling α_s . The three-momenta displayed in (2.1) refer to the e^+e^- c.m. frame. Top-quark production is analyzed in the continuum away from the $t\bar{t}$ threshold where perturbation theory is applicable. In the case of $Q = b$ we confine ourselves to $b\bar{b}$ production at the Z resonance.

The differential cross section to order α_s^2 of the reaction (2.1) was computed in [29] using the antenna subtraction framework. We extend these results to $t\bar{t}$ and $b\bar{b}$ production with polarized beams. A brief outline of the computational details is given at the end of this section.

We consider massless electrons. As usual the e^- and e^+ beam polarizations are described by the following polarizations projectors for the u and v spinors:

$$\begin{aligned} u(p_1, P_L) \otimes \bar{u}(p_1, P_L) &= \not{p}_1 (1 + P_L \gamma_5), \\ v(p_2, P_R) \otimes \bar{v}(p_2, P_R) &= \not{p}_2 (1 + P_R \gamma_5), \end{aligned} \quad (2.2)$$

where P_L is the left-handed polarization of the electron (+1 = fully left-handed, 0 = unpolarized, -1 = fully right-handed) and P_R is the right-handed polarization of the positron (+1, 0, -1 is fully-right-handed, unpolarized, and fully left-handed, respectively). Furthermore, we define

$$P_v = 1 + P_L P_R, \quad P_a = P_L + P_R \quad (2.3)$$

and for notational clarity, we use the notation $e_L^- \equiv P_L$ and $e_R^+ \equiv P_R$ in the following. For unpolarized beams, one has $P_v = 1, P_a = 0$. In the computations of the next sections we consider four benchmark polarization configurations listed in table 1.

Table 1: Benchmark polarizations of the e^- and e^+ beams used in the computations below and corresponding values of the polarization combinations (2.3).

e_L^-	e_R^+	P_v	P_a
-80%	+30%	0.76	-0.5
+80%	-30%	0.76	0.5
+80%	+30%	1.24	1.1
-80%	-30%	1.24	-1.1

The forward-backward asymmetry A_{FB} for the production of a massive quark Q is defined by

$$A_{\text{FB}} \equiv \frac{N_F - N_B}{N_F + N_B}, \quad (2.4)$$

where N_F (N_B) is the number of quarks Q produced in the forward (backward) direction. The identification of the forward and backward direction involves a choice of reference axis. The definition of the reference axis must be such that the resulting forward-backward asymmetry is an infrared safe (IR-safe) quantity so that it can be reliably calculated. The asymmetry A_{FB} is generated by those terms in the squared S-matrix elements of the reaction (2.1) that are odd under the interchange of Q and \bar{Q} (while the initial state is kept fixed).

The asymmetry A_{FB} can also be expressed conveniently in terms of the symmetric and antisymmetric cross section σ_S and σ_A for the inclusive production of the heavy quark Q , i.e.,

$$A_{\text{FB}} = \frac{\sigma_A}{\sigma_S} = \frac{\sigma_F - \sigma_B}{\sigma_F + \sigma_B}. \quad (2.5)$$

The σ_F and σ_B are the forward and backward cross sections, respectively.

To order α_s^2 the symmetric and antisymmetric cross sections receive the following perturbative contributions:

$$\sigma_{A,S} = \sigma_{A,S}^{(2,0)} + \sigma_{A,S}^{(2,1)} + \sigma_{A,S}^{(3,1)} + \sigma_{A,S}^{(2,2)} + \sigma_{A,S}^{(3,2)} + \sigma_{A,S}^{(4,2)} + \mathcal{O}(\alpha_s^3), \quad (2.6)$$

where the first number in the superscripts (i, j) denotes the number of final-state partons associated with the respective term and the second one the order of α_s . Inserting (2.6) into (2.5) we get the *unexpanded* A_{FB} to first and to second order in α_s :

$$A_{\text{FB}}(\alpha_s) = \frac{\sigma_A^{(2,0)} + \sigma_A^{(2,1)} + \sigma_A^{(3,1)}}{\sigma_S^{(2,0)} + \sigma_S^{(2,1)} + \sigma_S^{(3,1)}} \equiv A_{\text{FB}}^{\text{LO}} C_1, \quad (2.7)$$

$$A_{\text{FB}}(\alpha_s^2) = \frac{\sigma_A^{(2,0)} + \sigma_A^{(2,1)} + \sigma_A^{(3,1)} + \sigma_A^{(2,2)} + \sigma_A^{(3,2)} + \sigma_A^{(4,2)}}{\sigma_S^{(2,0)} + \sigma_S^{(2,1)} + \sigma_S^{(3,1)} + \sigma_S^{(2,2)} + \sigma_S^{(3,2)} + \sigma_S^{(4,2)}} \equiv A_{\text{FB}}^{\text{LO}} C_2, \quad (2.8)$$

where

$$A_{\text{FB}}^{\text{LO}} = \frac{\sigma_A^{(2,0)}}{\sigma_S^{(2,0)}} \quad (2.9)$$

is the forward-backward asymmetry at Born level. The factors C_1 and C_2 , defined by the respective ratio on the left-hand side of eq. (2.7) and (2.8), are the unexpanded first- and second-order QCD correction factors.

Taylor expanding eq. (2.7) to first order and eq. (2.8) to second order in α_s yields the *expanded* A_{FB} :

$$A_{\text{FB}}^{\text{NLO}} = A_{\text{FB}}^{\text{LO}} [1 + A_1] + \mathcal{O}(\alpha_s^2), \quad (2.10)$$

$$A_{\text{FB}}^{\text{NNLO}} = A_{\text{FB}}^{\text{LO}} [1 + A_1 + A_2] + \mathcal{O}(\alpha_s^3), \quad (2.11)$$

where A_1 and A_2 are the QCD corrections of $\mathcal{O}(\alpha_s)$ and $\mathcal{O}(\alpha_s^2)$, respectively.

$$A_1 = \sum_{i=2,3} \left[\frac{\sigma_A^{(i,1)}}{\sigma_A^{(2,0)}} - \frac{\sigma_S^{(i,1)}}{\sigma_S^{(2,0)}} \right], \quad (2.12)$$

$$A_2 = \sum_{i=2,3,4} \left[\frac{\sigma_A^{(i,2)}}{\sigma_A^{(2,0)}} - \frac{\sigma_S^{(i,2)}}{\sigma_S^{(2,0)}} \right] - \frac{\sigma_S^{(2,1)} + \sigma_S^{(3,1)}}{\sigma_S^{(2,0)}} A_1. \quad (2.13)$$

eqs. (2.10) and (2.11) are the expanded forms of the forward-backward asymmetry at NLO and NNLO QCD. The unexpanded and expanded first- and second-order forward-backward asymmetries differ by terms of order α_s^2 and order α_s^3 , respectively. The differences between the two forms may be considered as an estimate of the theory uncertainties.

With polarized beams, one can consider also the so-called polarized forward-backward asymmetry [51]:

$$A_{\text{pol,FB}} = \frac{1}{P} \frac{(\sigma_F(P) - \sigma_F(-P)) - (\sigma_B(P) - \sigma_B(-P))}{(\sigma_F(P) + \sigma_F(-P)) + (\sigma_B(P) + \sigma_B(-P))}, \quad (2.14)$$

where $P \equiv P_a/P_v$ (sometimes called the polarization degree of the e^+e^- system) with P_a, P_v defined in eqs.(2.3) and (2.2), and $\sigma_{F,B}(\pm P)$ is the heavy-quark cross section with beam polarization $\pm P$ in the forward hemisphere ($0 \leq \cos \theta \leq 1$) and backward hemisphere ($-1 \leq \cos \theta \leq 0$), respectively. In the case of $t\bar{t}$ production θ is the angle between the electron and the top quark. In the case of $b\bar{b}$ production at the Z peak, θ is the angle between the electron and the axis that defines the forward direction, cf. section 4. The variable $A_{\text{pol,FB}}$ combines data from different polarization configurations. We will see that, to lowest order in the electroweak couplings, the QCD correction factors to this observable remain exactly the same as in the unpolarized case. Unexpanded and expanded versions of this asymmetry can be obtained in complete analogy to (2.7), (2.8) and (2.10), (2.11), respectively, and we calculate both of them below.

In our computations we use for the on-shell top and b mass and other parameters [52] (we use the G_μ scheme):

$$m_t = 172.5 \text{ GeV}, \quad m_b = 4.78 \text{ GeV}, \quad m_Z = 91.1876 \text{ GeV}, \\ \sin^2 \theta_W = 0.2229, \quad \alpha_s(m_Z) = 0.11805, \quad \alpha_{em} = 0.00756. \quad (2.15)$$

For completeness, we sketch here our computational set-up that is a straightforward extension to polarized beams of the approach developed in [29, 44]. To the order of perturbation theory we are working the cross section of the reaction (2.1) receives contributions from the two-parton $Q\bar{Q}$ state (at Born level, to order α_s , and to order α_s^2), the three-parton state $Q\bar{Q}g$ (to order α_s and to order α_s^2), and the four-parton states $Q\bar{Q}gg, Q\bar{Q}q\bar{q}$, and above the $4Q$ threshold from $Q\bar{Q}Q\bar{Q}$ (to order α_s^2). In the case of $t\bar{t}$ production, all quarks q besides the top quark are taken to be massless, while in the case of $b\bar{b}$ production at the Z peak, the b -quark mass is taken to be massive.

As to the renormalization procedure used, as usual the QCD coupling $\alpha_s(\mu)$ is defined in the $\overline{\text{MS}}$ scheme at the chosen renormalization scale μ while the mass of the heavy quark is defined in the on-shell scheme.

We work to lowest order in the electroweak couplings. Thus, each of the just-mentioned various contributions $d\sigma^{(i,j)}$ to the differential $b\bar{b}$ cross section to order α_s^2 is given, at

arbitrary c.m. energy, by the sum of an s-channel γ and Z -boson contribution and a γZ interference term. The $d\sigma^{(i,j)}$ are of the form

$$d\sigma^{(i,j)} = \sum_{a=\gamma, Z, \gamma Z} F_a^{(j)} L_a^{\mu\nu} H_{a,\mu\nu}^{(i,j)} d\Phi_i. \quad (2.16)$$

The first index i in the superscript (i, j) labels the final state, i.e., $i = b\bar{b}, b\bar{b}g, b\bar{b}gg, b\bar{b}q\bar{q}$ ($q = u, d, s, c, b$). Here $d\Phi_i$ denotes the i -particle phase-space measure and $L_a^{\mu\nu}$ are the lepton tensors (with the boson propagators included) that contain, as compared to unpolarized beams, additional terms due to the polarization projectors (2.2). The tensors $H_{a,\mu\nu}^{(i,j)}$ are the antenna-subtracted, i.e., infrared finite parton tensors of order α_s^j [29]. The antenna subtraction terms that remove the soft and collinear divergences to order α_s^2 from the $Q\bar{Q}gg$ and $Q\bar{Q}q\bar{q}$ matrix elements were constructed in [53] and [54], respectively, while the subtraction terms for the $Q\bar{Q}g$ final state to order α_s^2 were determined in [55]. Thus the $d\sigma^{(i,j)}$ are finite by construction and, therefore, the Lorentz contractions and the phase-space integration in (2.16) can be done in $D = 4$ dimensions. The factors $F_a^{(j)}$ contain the electroweak couplings and the flux factor.

Each contribution (i, j) on the right-hand side of (2.16) is separated into a parity-even and -odd term. To lowest order in the electroweak couplings these terms determine the cross sections σ_S and σ_A that are symmetric and antisymmetric under the exchange of Q and \bar{Q} , respectively. For the numerical evaluation of the $d\sigma^{(i,j)}$ we use the approach described in detail in [29].

In section 4 we consider $b\bar{b}$ production exactly at the Z resonance. At this c.m. energy we neglect the s-channel γ and γZ interference contributions to the $d\sigma^{(i,j)}$ for determining the pure order α_s^2 QCD corrections to various FB b -quark asymmetries. In addition, we briefly discuss also the impact of the NLO electroweak corrections.

3 Asymmetries for top quarks

We consider in this section $t\bar{t}$ production to $\mathcal{O}(\alpha_s^2)$ for c.m. energies 380 GeV, 400 GeV, 500 GeV, and 700 GeV. The latter c.m. energy is above threshold for $4t$ production. However, the $4t$ final state, whose matrix element is ultraviolet and infrared finite at this order of perturbation theory, makes only a very small contribution to the cross section at this energy. Moreover, the $4t$ production can be well separated experimentally from the other $t\bar{t} + X$ final states. Therefore, we do not take this contribution into account in the results to be presented below. The various contributions to $t\bar{t}$ production are conveniently classified as follows: flavor non-singlet (where the virtual Z and γ directly couple to the external $t\bar{t}$), flavor singlet (where $t\bar{t}$ is produced by a virtual gluon), and triangle or interference terms [42, 44].

We use the top-quark direction of flight in the e^+e^- c.m. frame as reference axis for defining the forward and backward hemisphere. This axis is infrared- and collinear-safe. The top-direction of flight can be reconstructed for instance with lepton plus jets events (or from all jets events) from $t\bar{t}$ decay.

Tables 2, 3, 4, and 5 contain our results for the symmetric $t\bar{t}$ cross section, for the forward-backward asymmetry at LO, and the corrections A_1 and A_2 to $A_{\text{FB}}^{\text{LO}}$ at NLO and NNLO QCD in expanded form, both for unpolarized beams and the polarization configurations listed in table 1, for the above c.m. energies. The corresponding unexpanded NLO and NNLO QCD correction factors C_1 and C_2 are listed in table 6. The numbers for the QCD corrections given in these tables were obtained by setting the renormalization scale $\mu = \sqrt{s}$. The numbers in super- and subscript correspond to the changes that result from setting the scale to $\mu = 2\sqrt{s}$ and $\mu = \sqrt{s}/2$, respectively. The results for the scale variations are derived by first obtaining the values of the symmetric and antisymmetric cross sections σ_S , σ_A , respectively, at $\mu = 2\sqrt{s}$ and $\mu = \sqrt{s}/2$ by means of the renormalization-group equation from which the scale uncertainties for the various quantities listed in the aforementioned tables are composed. For the unexpanded A_{FB} and the corresponding C_1, C_2 coefficients being defined as ratios, it is expected that there is a cancellation between the scale dependence of the symmetric and antisymmetric cross sections if one chooses to vary both simultaneously. Consequently, the scale uncertainties for these ratios are relatively small and may not display the usual improvement when the higher order perturbative corrections are included, see table 6. Alternatively, one may choose to set the scale of σ_S different from that of σ_A to obtain a more conservative estimate for the scale uncertainties of these ratios. However, we refrain from listing in these tables the scale uncertainties derived with these alternative conventions, both for the sake of not over-loading the tables and also because their magnitudes are comparable to that of the scale uncertainties of σ_S , which are provided. On the other hand, this feature is not exhibited in the QCD correction factors A_1, A_2 related to the expanded A_{FB} , and one does observe the usual improvement when the higher order perturbative corrections are included, see e.g. tables 2, 3, 4, and 5. In particular, the improvement becomes better when the total energy of the collision is increased, which is expected because the perturbative convergences improves away from the pair-production threshold.

Moreover, for fixed c.m. energy, the QCD correction terms to $A_{\text{FB}}^{\text{LO}}$ show a marginal dependence on the beam polarization. In order to quantify the variations of the expansion terms A_1, A_2 with the beam polarization, we introduce the ratio

$$R_i(e_L^-, e_R^+) = \frac{A_i(e_L^-, e_R^+) - A_i(0, 0)}{A_i(0, 0)}, \quad (3.1)$$

where $A_i(e_L^-, e_R^+)$ ($i = 1, 2$) denote the i -th order QCD correction terms for the electron and positron polarization configurations, specified by e_L^- and e_R^+ , respectively, as given in table 1, and in particular $A_i(0, 0)$ are the QCD correction terms for unpolarized beams. Furthermore, we use

$$R_i^{\text{max}} \equiv \max[R_i(e_L^-, e_R^+)] - \min[R_i(e_L^-, e_R^+)] = \frac{\max[A_i(e_L^-, e_R^+)] - \min[A_i(e_L^-, e_R^+)]}{A_i(0, 0)} \quad (3.2)$$

for signifying the maximal spread of A_i in relation to the correction for unpolarized beams. The meaning of the max/min operation is as usual, for example, $\max/\min[A_i(e_L^-, e_R^+)]$ denotes the maximal/minimal value of the QCD correction term $A_i(e_L^-, e_R^+)$ for all beam

Table 2: Top-quark pair production at $\sqrt{s} = 380$ GeV for unpolarized beams and the polarization configurations of table 1. The renormalization scale is chosen to be $\mu = \sqrt{s}$, with the scale uncertainties of the symmetric cross sections σ_S given by the shifts in the super- and subscripts (corresponding to scales $\mu = 2\sqrt{s}$ and $\mu = \sqrt{s}/2$, respectively). Symmetric cross sections σ_S in units of pb, A_{FB} to LO, and the terms A_1 , A_2 defined in (2.10), (2.11) that yield the expanded A_{FB} , respectively, to NLO and NNLO QCD. The numbers for A_1 , A_2 and their scale variations are given in the unit of 10^{-2} .

Beam polarization (e_L^-, e_R^+)	LO		NLO		NNLO	
	σ_S [pb]	$A_{\text{FB}}^{\text{LO}}$	σ_S [pb]	A_1 [10^{-2}]	σ_S [pb]	A_2 [10^{-2}]
(0, 0)	0.58477	0.2342	$0.78874_{-0.01741}^{+0.01484}$	$3.67_{-0.267}^{+0.313}$	$0.85037_{-0.01002}^{+0.01009}$	$2.92_{-0.168}^{+0.188}$
(-80%, +30%)	0.32039	0.2549	$0.43232_{-0.00955}^{+0.00814}$	$3.62_{-0.263}^{+0.309}$	$0.46633_{-0.00553}^{+0.00556}$	$2.86_{-0.163}^{+0.183}$
(+80%, -30%)	0.56846	0.2226	$0.76657_{-0.01691}^{+0.01441}$	$3.70_{-0.270}^{+0.316}$	$0.82623_{-0.00977}^{+0.00970}$	$2.95_{-0.170}^{+0.191}$
(+80%, +30%)	0.99800	0.2196	$1.34571_{-0.02968}^{+0.02530}$	$3.71_{-0.270}^{+0.317}$	$1.45035_{-0.01701}^{+0.01714}$	$2.96_{-0.171}^{+0.192}$
(-80%, -30%)	0.45224	0.2664	$0.61037_{-0.01350}^{+0.01151}$	$3.59_{-0.261}^{+0.306}$	$0.65856_{-0.00784}^{+0.00788}$	$2.82_{-0.160}^{+0.180}$

Table 3: Top-quark pair production at $\sqrt{s} = 400$ GeV. The meaning of the variables is as in table 2.

Beam polarization (e_L^-, e_R^+)	LO		NLO		NNLO	
	σ_S [pb]	$A_{\text{FB}}^{\text{LO}}$	σ_S [pb]	A_1 [10^{-2}]	σ_S [pb]	A_2 [10^{-2}]
(0, 0)	0.62928	0.2845	$0.79311_{-0.01389}^{+0.01186}$	$3.39_{-0.245}^{+0.287}$	$0.83400_{-0.00648}^{+0.00685}$	$2.31_{-0.101}^{+0.106}$
(-80%, +30%)	0.34658	0.3083	$0.43708_{-0.00767}^{+0.00655}$	$3.31_{-0.240}^{+0.281}$	$0.45987_{-0.00362}^{+0.00381}$	$2.25_{-0.097}^{+0.102}$
(+80%, -30%)	0.60992	0.2710	$0.76845_{-0.01344}^{+0.01147}$	$3.43_{-0.248}^{+0.291}$	$0.80780_{-0.00623}^{+0.00660}$	$2.35_{-0.104}^{+0.109}$
(+80%, +30%)	1.06997	0.2675	$1.34797_{-0.02357}^{+0.02012}$	$3.44_{-0.249}^{+0.292}$	$1.41687_{-0.01091}^{+0.01156}$	$2.36_{-0.104}^{+0.109}$
(-80%, -30%)	0.49064	0.3215	$0.61895_{-0.01088}^{+0.00929}$	$3.27_{-0.237}^{+0.277}$	$0.65144_{-0.00516}^{+0.00543}$	$2.21_{-0.095}^{+0.099}$

Table 4: Top-quark pair production at $\sqrt{s} = 500$ GeV. The meaning of the variables is as in table 2.

Beam polarization (e_L^-, e_R^+)	LO		NLO		NNLO	
	σ_S [pb]	$A_{\text{FB}}^{\text{LO}}$	σ_S [pb]	A_1 [10^{-2}]	σ_S [pb]	A_2 [10^{-2}]
(0, 0)	0.55084	0.4169	$0.62006_{-0.00571}^{+0.00489}$	$2.26_{-0.159}^{+0.186}$	$0.63038_{-0.00147}^{+0.00187}$	$1.16_{-0.014}^{+0.004}$
(-80%, +30%)	0.30850	0.4458	$0.34762_{-0.00323}^{+0.00276}$	$2.14_{-0.151}^{+0.177}$	$0.35362_{-0.00086}^{+0.00108}$	$1.10_{-0.013}^{+0.003}$
(+80%, -30%)	0.52877	0.4001	$0.59488_{-0.00545}^{+0.00467}$	$2.32_{-0.164}^{+0.192}$	$0.60456_{-0.00138}^{+0.00176}$	$1.20_{-0.015}^{+0.004}$
(+80%, +30%)	0.92534	0.3957	$1.04086_{-0.00953}^{+0.00816}$	$2.34_{-0.165}^{+0.193}$	$1.05771_{-0.00239}^{+0.00307}$	$1.21_{-0.015}^{+0.004}$
(-80%, -30%)	0.44074	0.4614	$0.49689_{-0.00463}^{+0.00397}$	$2.08_{-0.147}^{+0.172}$	$0.50564_{-0.00126}^{+0.00157}$	$1.07_{-0.012}^{+0.003}$

polarization configurations e_L^-, e_R^+ considered in this paper. The same remark applies to the notation $\max/\min[R_i(e_L^-, e_R^+)]$. The values of R_i^{\max} are given in table 7 for the four

Table 5: Top-quark pair production at $\sqrt{s} = 700$ GeV. The meaning of the variables is as in table 2, except that the numbers for A_2 and its scale variations are given in the unit of 10^{-3} .

Beam polarization (e_L^-, e_R^+)	LO		NLO		NNLO	
	σ_S [pb]	$A_{\text{FB}}^{\text{LO}}$	σ_S [pb]	A_1 [10^{-2}]	σ_S [pb]	A_2 [10^{-3}]
(0, 0)	0.32344	0.5144	$0.34560_{-0.00176}^{+0.00151}$	$0.90_{-0.061}^{+0.071}$	$0.34759_{-0.00024}^{+0.00040}$	$4.6_{-0.048}^{+0.009}$
(−80%, +30%)	0.18367	0.5440	$0.19644_{-0.00101}^{+0.00087}$	$0.79_{-0.054}^{+0.063}$	$0.19766_{-0.00015}^{+0.00024}$	$4.2_{-0.058}^{+0.027}$
(+80%, −30%)	0.30796	0.4968	$0.32887_{-0.00166}^{+0.00143}$	$0.96_{-0.065}^{+0.076}$	$0.33068_{-0.00021}^{+0.00037}$	$4.8_{-0.043}^{+0.001}$
(+80%, +30%)	0.53779	0.4922	$0.57422_{-0.00289}^{+0.00249}$	$0.97_{-0.066}^{+0.077}$	$0.57734_{-0.00037}^{+0.00064}$	$4.9_{-0.041}^{+0.004}$
(−80%, −30%)	0.26435	0.5597	$0.28288_{-0.00147}^{+0.00126}$	$0.74_{-0.050}^{+0.059}$	$0.28469_{-0.00022}^{+0.00035}$	$4.0_{-0.063}^{+0.037}$

Table 6: The factors C_1 , C_2 defined in eq. (2.7) and eq. (2.8) that yield the unexpanded A_{FB} to NLO and NNLO QCD. The numbers for C_1 , C_2 and their scale variations are given in the unit of 10^{-2} .

Beam polarization (e_L^-, e_R^+)		(0, 0)	(−80%, +30%)	(+80%, −30%)	(+80%, +30%)	(−80%, −30%)
380 GeV	$C_1 - 1$ [10^{-2}]	$2.72_{-0.149}^{+0.170}$	$2.68_{-0.148}^{+0.169}$	$2.75_{-0.152}^{+0.168}$	$2.75_{-0.152}^{+0.169}$	$2.66_{-0.145}^{+0.161}$
	$C_2 - 1$ [10^{-2}]	$5.41_{-0.360}^{+0.435}$	$5.32_{-0.355}^{+0.429}$	$5.47_{-0.367}^{+0.437}$	$5.48_{-0.368}^{+0.440}$	$5.26_{-0.352}^{+0.418}$
400 GeV	$C_1 - 1$ [10^{-2}]	$2.69_{-0.155}^{+0.180}$	$2.63_{-0.149}^{+0.177}$	$2.72_{-0.160}^{+0.179}$	$2.73_{-0.158}^{+0.180}$	$2.59_{-0.151}^{+0.174}$
	$C_2 - 1$ [10^{-2}]	$4.96_{-0.316}^{+0.374}$	$4.84_{-0.305}^{+0.364}$	$5.03_{-0.323}^{+0.379}$	$5.05_{-0.322}^{+0.381}$	$4.77_{-0.304}^{+0.356}$
500 GeV	$C_1 - 1$ [10^{-2}]	$2.01_{-0.129}^{+0.146}$	$1.90_{-0.121}^{+0.136}$	$2.06_{-0.133}^{+0.152}$	$2.08_{-0.133}^{+0.152}$	$1.85_{-0.116}^{+0.136}$
	$C_2 - 1$ [10^{-2}]	$3.23_{-0.178}^{+0.200}$	$3.07_{-0.168}^{+0.193}$	$3.33_{-0.183}^{+0.206}$	$3.36_{-0.183}^{+0.208}$	$2.98_{-0.161}^{+0.184}$
700 GeV	$C_1 - 1$ [10^{-2}]	$0.84_{-0.055}^{+0.060}$	$0.74_{-0.050}^{+0.053}$	$0.90_{-0.057}^{+0.066}$	$0.91_{-0.058}^{+0.065}$	$0.69_{-0.044}^{+0.051}$
	$C_2 - 1$ [10^{-2}]	$1.32_{-0.068}^{+0.075}$	$1.17_{-0.063}^{+0.072}$	$1.40_{-0.069}^{+0.082}$	$1.42_{-0.071}^{+0.079}$	$1.10_{-0.058}^{+0.066}$

benchmark polarizations and the c.m. energies considered. For instance, for $\sqrt{s} = 500$ GeV A_1, A_2 become maximal for the polarization configuration $e_L^- = 80\%$, $e_R^+ = 30\%$ where $R_1(80\%, 30\%) = 4.63\%$, $R_2(80\%, 30\%) = 5.17\%$, and the minimal values are taken at $e_L^- = -80\%$, $e_R^+ = -30\%$ where $R_1(80\%, 30\%) = -7.7\%$, $R_2(80\%, 30\%) = -8.0\%$. Although the relative spreads listed in table 7 appear to be quite large, one should notice that in absolute terms they amount to changes of the NLO and NNLO QCD correction factors for unpolarized beams, $(1 + A_1)$ and $(1 + A_1 + A_2)$, respectively, of only a few per mille. The projected statistical uncertainty of the polarized $t\bar{t}$ cross section and top forward-backward asymmetry at future high-energy high-luminosity electron-positron colliders was estimated to be at the level of a few per mille, c.f. [56, 57], hence the effect of the beam polarization on the QCD correction factors are comparable to that. With the results for the symmetric $t\bar{t}$ cross section and the forward-backward asymmetry with polarized beams presented in tables 2, 3, 4, the corresponding theoretical uncertainties can be reduced.

The dependence on the beam polarization arises because the final-state quark is massive and because of the coherent contributions of the Z - and γ -exchange contributions.

Table 7: The ratio R_i^{\max} for different c.m. energies.

\sqrt{s} [GeV]	380	400	500	700
R_1^{\max}	3.4%	5.0%	12.3%	26.0%
R_2^{\max}	4.6%	6.2%	13.3%	20.3%

Specifically, as far as A_{FB} in its expanded form is concerned, the beam-polarization dependence of the A_i originate from the ratios of the symmetric cross sections (that depend both on P_v and P_a) in eqs. (2.12), (2.13). The dependence of the antisymmetric cross sections on the beam polarization is just an overall factor that cancels in the respective ratios in eqs. (2.12), (2.13). In addition, starting at NNLO QCD, there are also flavor singlet contributions that supply additional polarization dependence. However, for $t\bar{t}$ production at energies considered here the singlet contributions are tiny (of order 10^{-4} relative to $A_{\text{FB}}^{\text{LO}}$). In other words, $t\bar{t}$ production at these energies is completely dominated by the flavor non-singlet corrections. In the limit of extremely high energies, $m_t/\sqrt{s} \rightarrow 0$, the polarization dependence of the A_i from the non-singlet contribution disappears.

We investigated also the dependence of A_1, A_2 on the uncertainty of the value of top-quark pole mass. Varying $\delta m_t = \pm 0.7$ GeV we found that the resulting variation of these correction terms given in tables 2, 3, 4, and 5 is less than 1%.

The top-quark A_{FB} was computed before in [28, 29] to NNLO QCD for unpolarized beams at $\sqrt{s} = 500$ GeV. Using the same values of the input parameters that were used in these papers we checked that we agree with their results.

The above forward-backward asymmetries are obtained from the respective distribution of the top-quark polar angle $\theta_t = \angle(\mathbf{k}_1, \mathbf{p}_1)$ in the e^+e^- c.m. frame, cf. eq. (2.1). Here we restrict ourselves to discuss its distribution for $t\bar{t}$ production at 500 GeV. In the plots below we use the notation $d\sigma_{\text{NLO}} = d\sigma_{\text{LO}} + d\sigma_1$ and $d\sigma_{\text{NNLO}} = d\sigma_{\text{LO}} + d\sigma_1 + d\sigma_2$ for the differential cross section at NLO and NNLO QCD, respectively. The upper panel of the plot in figure 1a displays the distribution of $\cos\theta_t$ at LO, NLO, and NNLO QCD for unpolarized beams. The panel in the middle of the plot shows that the inclusion of the order α_s^2 correction significantly reduces the dependence of this distribution on variations of the scale μ . The lower panel exhibits the ratio $d\sigma_1/d\sigma_{\text{LO}}$ and $d\sigma_2/d\sigma_{\text{LO}}$ for $\mu = \sqrt{s}$. Both the order α_s and order α_s^2 corrections follow the same pattern as the leading-order distribution: they are larger in the top-quark forward direction and thus increase the forward-backward asymmetry. The upper panel of the plot in figure 1b displays, at $\sqrt{s} = 500$ GeV and LO QCD, the ratios of the $\cos\theta_t$ distributions with and without polarized beams. The lower panel shows the ratios of the $\cos\theta_t$ distributions $[(d\sigma_{\text{NNLO}}^{\text{pol}}/d\sigma_{\text{LO}}^{\text{pol}})/(d\sigma_{\text{NNLO}}/d\sigma_{\text{LO}})] - 1$ for the various polarization configurations for $\mu = \sqrt{s}$.

Finally we consider the polarized forward-backward asymmetry $A_{\text{pol,FB}}$ defined in (2.14). It is independent of the polarization configurations of table 1. Moreover, for all c.m. energies, the QCD correction terms $A_1^{\text{pol,FB}}$ and $A_2^{\text{pol,FB}}$ to the leading-order polarized forward-backward asymmetry are the same as the respective unpolarized terms A_1, A_2 .

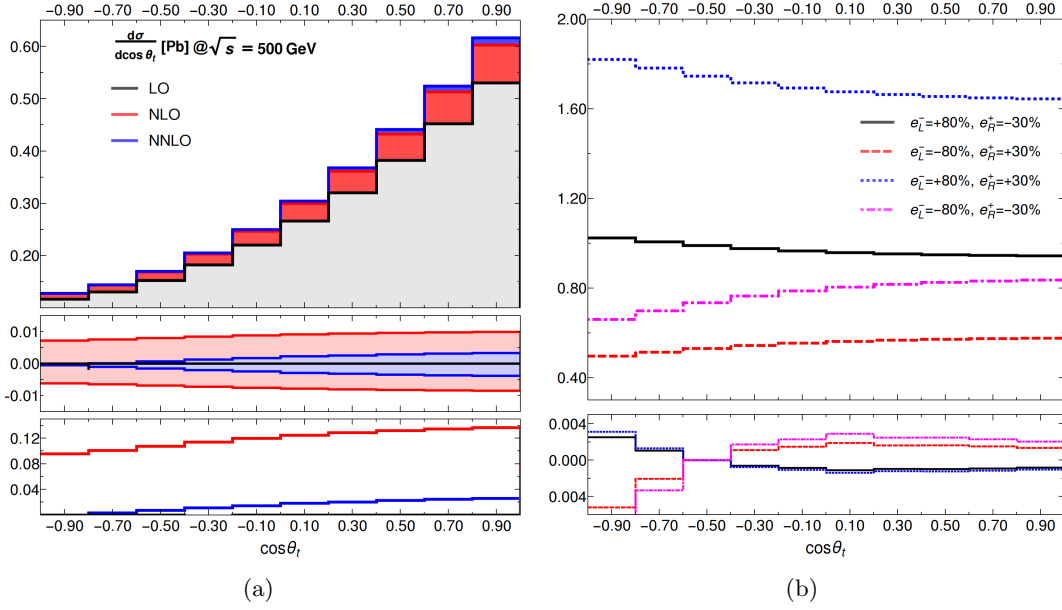


Figure 1: (a) The upper panel shows the $\cos\theta_t$ distribution for unpolarized beams at LO(grey, lower steps), NLO(red, steps in the middle), and NNLO QCD(blue, upper steps) for $\mu = \sqrt{s} = 500$ GeV. The panel in the middle displays the scale variations $[d\sigma_{\text{NLO}}(\mu')/d\sigma_{\text{NLO}}(\mu = \sqrt{s})] - 1$ (red, wide band) and $[d\sigma_{\text{NNLO}}(\mu')/d\sigma_{\text{NNLO}}(\mu = \sqrt{s})] - 1$ (blue, narrow band) of the first and second order QCD corrections, where $\sqrt{s}/2 < \mu' < 2\sqrt{s}$. The lower panel shows the ratio $d\sigma_1/d\sigma_{\text{LO}}$ (red, upper steps) and $d\sigma_2/d\sigma_{\text{LO}}$ (blue, lower steps) for $\mu = \sqrt{s}$. (b) The upper panel shows the LO QCD ratios of the $\cos\theta_t$ distributions with polarized and unpolarized beams at $\sqrt{s} = 500$ GeV. The lower panels display the ratios of the $\cos\theta_t$ distributions $[(d\sigma_{\text{NNLO}}^{\text{pol}}/d\sigma_{\text{LO}}^{\text{pol}})/(d\sigma_{\text{NNLO}}/d\sigma_{\text{LO}})] - 1$ for the various polarization configurations for $\mu = \sqrt{s}$. The coding is the same as in the upper panel.

The respective ratios $A_{\text{FB}}/A_{\text{pol,FB}}$ are given in table 8. They vary slightly with the c.m. energy due to the slight change in the relative weights of the coherent Z -boson and photon exchange amplitudes.

Table 8: The ratio of the polarized forward-backward asymmetry and the asymmetry for unpolarized beams for top-quark pair production at various c.m. energies. The respective ratio at \sqrt{s} holds for all polarization configurations of table 1 and is valid at LO, NLO, and NNLO QCD.

\sqrt{s} [GeV]	380	400	500	700
$A_{\text{FB}}/A_{\text{pol,FB}}$	3.053	3.065	3.103	3.136

4 Asymmetries for b -quark pair production at the Z peak

Next we consider the production of $b\bar{b}$ pairs at the Z resonance to NNLO QCD and to lowest order in the electroweak couplings, i.e., $b\bar{b}$ production by a virtual photon is not taken into account. The b quark is taken to be massive, with an on-shell mass value given in (2.15) where also the other SM parameter values relevant for the calculations below are listed.

As in the case of top-quark production we consider $b\bar{b}$ production both by unpolarized and polarized e^+ and e^- beams, with polarization configurations as given in table 1.

We will compute the b -quark A_{FB} for several definitions of the forward and backward hemispheres. First we will use the b -quark direction of flight and the oriented thrust axis for defining these hemispheres. If the b -quark direction of flight is chosen then the hemispheres are separated according to $\cos\theta_b$ being larger or smaller than zero, where $\theta_b = \angle(\mathbf{k}_1, \mathbf{p}_1)$, cf. eq. (2.1). Because an accurate determination of the b -quark flight direction is difficult, experimental analyses in the past often used the thrust axis as reference axis. For a given n -parton event described by a collection of final-state four-momenta $\{k_i\}_{i=1}^n$ (related by momentum conservation), the thrust axis is the direction \mathbf{n}_T that maximizes the thrust T defined by [58–60]:

$$T = \max_{\mathbf{n}_T} \frac{\sum_{i=1}^n |\mathbf{k}_i \cdot \mathbf{n}_T|}{\sum_{i=1}^n |\mathbf{k}_i|}, \quad |\mathbf{n}_T| = 1. \quad (4.1)$$

The orientation of the thrust axis is fixed by requiring $\mathbf{n}_T \cdot \mathbf{k}_1 > 0$. If the thrust axis is chosen as reference axis, the forward and backward hemispheres are discriminated by the sign of $\cos\theta_T$ where $\theta_T = \angle(\mathbf{n}_T, \mathbf{p}_1)$.

We recall that the various contributions to the inclusive b -quark cross section and, in particular, to the b -quark FB asymmetry at NNLO QCD can be classified into flavor non-singlet, flavor singlet, and interference or triangle terms. (For details see, e.g., [44].) The contribution from the $b\bar{b}b\bar{b}$ final state deserves special mention. In the calculation of the b -quark FB asymmetry, i.e., in the calculation of the forward and backward cross sections σ_S and σ_A , we have the following situations: i) both b quarks are in the forward (backward) direction, thus they contribute both to σ_F (σ_B). ii) one b quark is forward, the other one backward, thus there is a contribution both to σ_F and σ_B .

Table 9 shows, for the b -quark axis definition of the forward and backward hemispheres, our results for unpolarized beams and for the polarization configurations of table 1. The cross sections σ_S at LO, NLO, and NNLO QCD are given for the scale choice $\mu = m_Z$. Apart from the Born level $A_{\text{FB}}^{\text{LO}}$ also the first- and second-order expansion terms are displayed, including the changes that result from varying μ between $m_Z/2$ and $2m_Z$. For brevity we display here and in the tables below only the QCD corrections to $A_{\text{FB}}^{\text{LO}}$ in expanded form.

As the numbers in this table show, A_1 is, in contrast to the case of the top quark, independent of the beam polarization. This is because only the Z -boson exchange is taken into account. The polarization dependence of A_2 arises solely from the flavor singlet

Table 9: Production of $b\bar{b}$ at the Z peak for unpolarized beams and the polarization configurations of table 1. Here the FB asymmetry is defined with respect to the b -quark axis. Symmetric cross sections σ_S in units of pb, A_{FB} to LO and the terms A_1 , A_2 defined in (2.10), (2.11) that yield the expanded A_{FB} to NLO and NNLO QCD. The parameters listed in eq. (2.15) are used. The renormalization scale is chosen to be $\mu = m_Z$. The numbers in superscript (subscript) refer to the changes if $\mu = 2m_Z$ ($\mu = m_Z/2$) is chosen. The numbers for A_1 , A_2 and their scale variations are given in the unit of 10^{-2} .

Beam polarization e_L^-, e_R^+	LO		NLO		NNLO	
	σ_S [pb]	$A_{\text{FB}}^{\text{LO}}$	σ_S [pb]	A_1 [10^{-2}]	σ_S [pb]	A_2 [10^{-2}]
(0, 0)	8747.4	0.1512	$9122.8_{-35.5}^{+44.1}$	$-2.92_{-0.343}^{+0.277}$	$9164.8_{-12.4}^{+7.7}$	$-1.28_{-0.008}^{+0.046}$
(-80%, +30%)	5710.7	-0.3644	$5955.8_{-23.2}^{+28.8}$	$-2.92_{-0.343}^{+0.277}$	$5990.6_{-9.4}^{+6.9}$	$-1.35_{-0.005}^{+0.028}$
(+80%, -30%)	7585.3	0.5394	$7910.9_{-30.8}^{+38.2}$	$-2.92_{-0.343}^{+0.277}$	$7939.9_{-9.4}^{+4.8}$	$-1.16_{-0.031}^{+0.077}$
(+80%, +30%)	12908.8	0.6531	$13462.8_{-52.4}^{+65.0}$	$-2.92_{-0.343}^{+0.277}$	$13508.5_{-15.3}^{+7.3}$	$-1.12_{-0.036}^{+0.085}$
(-80%, -30%)	8784.7	-0.5862	$9161.7_{-35.7}^{+44.2}$	$-2.92_{-0.343}^{+0.277}$	$9220.1_{-15.3}^{+11.8}$	$-1.42_{-0.016}^{+0.016}$

contributions. Defining a quantity $R_2^{\text{max}}(b)$ in analogy to eq. (3.2) in order to quantify the maximal spread of A_2 due to beam polarization one gets $|R_2^{\text{max}}(b)| = 23\%$. As already found in [44] for unpolarized beams, the order α_s^2 corrections are quite large for all polarization configurations. From table 9 we get $40\% \leq A_2/A_1 \leq 48\%$.

The flavor non-singlet corrections A_2^{ns} of order α_s^2 that contain the neutral current couplings of the b quarks, are independent of beam polarization. For the quark axis definition of the asymmetry we get $A_2^{\text{ns}} = -0.0084$ (for $\mu = m_Z$) that amounts to 65% of the total correction A_2 .

Table 10 contains the analogous information for the definition of the forward and backward hemispheres with respect to the oriented thrust axis. Using again eq. (3.2) to quantify the maximal spread of A_2 for the above beam polarizations, we get here $|R_2^{\text{max}}(b)| = 27\%$. The ratio A_2/A_1 varies between 33% and 43% which is somewhat smaller than in the case of the b -quark axis definition.

Table 10: Same as table 9, but here the asymmetry is defined with respect to the thrust axis.

Beam polarization e_L^-, e_R^+	LO		NLO		NNLO	
	σ_S [pb]	$A_{\text{FB}}^{\text{LO}}$	σ_S [pb]	A_1 [10^{-2}]	σ_S [pb]	A_2 [10^{-2}]
(0, 0)	8747.4	0.1512	9122.8	$-2.88_{-0.338}^{+0.273}$	9164.8	$-1.11_{-0.037}^{+0.085}$
(-80%, +30%)	5710.7	-0.3644	5955.8	$-2.88_{-0.338}^{+0.273}$	5990.6	$-1.19_{-0.022}^{+0.064}$
(+80%, -30%)	7585.3	0.5394	7910.9	$-2.88_{-0.338}^{+0.273}$	7939.9	$-0.99_{-0.058}^{+0.115}$
(+80%, +30%)	12908.8	0.6531	13462.8	$-2.88_{-0.338}^{+0.273}$	13508.5	$-0.96_{-0.064}^{+0.122}$
(-80%, -30%)	8784.7	-0.5862	9161.7	$-2.88_{-0.338}^{+0.273}$	9220.1	$-1.25_{-0.338}^{+0.049}$

The $b\bar{b}b\bar{b}$ final state has a distinctive experimental signature. Depending on the b -tagging efficiency it could, in principle, be separated from the other final states. In order to assess the contribution of the $b\bar{b}b\bar{b}$ final state, we compute now A_{FB} without including these events. This changes σ_S at NNLO QCD and the expansion term A_2 . The resulting values for these quantities are given in table 11 for unpolarized beams. Comparing with the numbers in tables 9 and 10 shows that A_2 is reduced in magnitude by 10% and 11% in the case of the b -quark axis and thrust axis definition, respectively.

Table 11: The $b\bar{b}$ cross sections σ_S in units of pb at NNLO QCD at the Z peak for unpolarized beams and $\mu = m_Z$ without the contribution from the $b\bar{b}b\bar{b}$ final state and the resulting expansion terms A_2 for the quark-axis and thrust-axis definition of the FB asymmetry. The numbers for A_1 , A_2 and their scale variations are given in the unit of 10^{-2} .

quark axis		thrust axis	
σ_S [pb]	A_2 [10^{-2}]	σ_S [pb]	A_2 [10^{-2}]
9148.0	$-1.17^{+0.074}_{-0.028}$	9148.0	$-0.99^{+0.113}_{-0.057}$

The forward-backward asymmetry at the Z resonance were computed in [44] with respect to the b -quark direction and the oriented thrust direction, for massive b quarks and unpolarized beams, with input parameters that differ somewhat from the ones used here. We agree with these results.

Next we consider jets and use the direction of the b jet to define the forward and backward hemispheres and compute A_{FB} . We use the Durham [49] and the flavor- k_T [50] jet clustering algorithms. In applications to flavored massless quark jets, the Durham algorithm is infrared-unsafe at order α_s^2 while the flavor- k_T algorithm is infrared safe by construction [50]. However, as we consider massive b quarks, also the Durham algorithm allows for an infrared-safe definition of a b jet. One assigns the flavor number +1 (−1) to a b quark (\bar{b} quark) and flavor number 0 to the other quarks and the gluon. Flavor numbers are added. If two b quarks (b and \bar{b}) are combined the resulting pseudoparticle has flavor number 2 (0). We recall the respective distance measure between every pair of partons (resp. pseudoparticles) i, j :

$$y_{ij}^X = (1 - \cos \theta_{ij}) \frac{2r_X}{s}, \quad (4.2)$$

where θ_{ij} is the angle between (pseudo)particles i and j . The Durham algorithm is defined by $r_D = \min(E_i^2, E_j^2)$, where E_i is the energy of (pseudo)particle i , while in the case of the flavor- k_T algorithm

$$r_F = \begin{cases} \max(E_i^2, E_j^2), & \text{if softer of } i, j \text{ is flavored,} \\ \min(E_i^2, E_j^2), & \text{if softer of } i, j \text{ is flavorless.} \end{cases} \quad (4.3)$$

For recombining i and j whose distance y_{ij}^X is smaller than a specified jet resolution parameter y_{cut} we use the E scheme that sums the four-momenta ($k_{(ij)} = k_i + k_j$).

Table 12 contains, for unpolarized beams, our results for the bottom quark cross section σ_S to order α_s^2 where the forward and backward hemispheres are defined with respect to the b -jet direction, both for the flavor- k_T and the Durham algorithm with a sequence of jet resolution parameters y_{cut} . Moreover, the NLO and NNLO QCD correction terms to A_{FB}^{LO} are given. The term A_1 (A_2) receives contributions from two- and three-jet (two-, three-, and four-jet) events with b -flavor number larger than zero. Jet events with b -flavor number zero are not taken into account; in particular, they are not included in σ_S . That is why the numbers for σ_S differ for different jet algorithms.

With less stringent jet resolution parameter y_{cut} the magnitudes of the QCD correction factors to the inclusive b -jet A_{FB} become smaller. The order α_s^2 correction terms A_2 decrease relative to A_1 with increasing y_{cut} as the ratios A_2/A_1 listed in table 13 show. For $y_{cut} \geq 0.1$ these ratios become smaller compared to A_2/A_1 in the case of b -quark and thrust axis definition of A_{FB} , cf. Tables 9, 10.

From the numbers in table 14 we deduce that using the Durham (flavor- k_T) algorithm the contribution of the $b\bar{b}b\bar{b}$ final state to A_2 is about 6% (8%) for $y_{cut} = 0.01$ and decreases to about 3% (6%) for $y_{cut} = 0.15$.

Table 12: Production of $b\bar{b}$ at the Z peak for unpolarized beams. Here the FB asymmetry is defined with respect to the b -jet axis and two different jet algorithms are used. Symmetric cross sections σ_S in units of pb, A_{FB} to LO and the terms A_1 , A_2 defined in (2.10), (2.11) that yield the expanded A_{FB} to NLO and NNLO QCD. The parameters listed in eq. (2.15) are used. The renormalization scale is chosen to be $\mu = m_Z$. The numbers for A_1 , A_2 and their scale variations are given in the unit of 10^{-2} .

Jet algorithms (y_{cut})	LO		NLO		NNLO	
	σ_S [pb]	A_{FB}^{LO}	σ_S [pb]	A_1 [10^{-2}]	σ_S [pb]	A_2 [10^{-2}]
Flavor k_T , 0.01	8747.4	0.1512	9120.7	$-2.88^{+0.037}_{+0.021}$	9150.4	$-1.09^{+0.216}_{-0.303}$
Flavor k_T , 0.05	8747.4	0.1512	9111.4	$-2.67^{+0.034}_{+0.020}$	9121.4	$-0.83^{+0.167}_{-0.236}$
Flavor k_T , 0.10	8747.4	0.1512	9098.2	$-2.42^{+0.031}_{+0.018}$	9097.7	$-0.68^{+0.138}_{-0.195}$
Flavor k_T , 0.15	8747.4	0.1512	9082.8	$-2.18^{+0.028}_{+0.016}$	9075.3	$-0.59^{+0.120}_{-0.169}$
Durham, 0.01	8747.4	0.1512	9100.2	$-2.58^{+0.033}_{+0.019}$	9112.1	$-0.87^{+0.174}_{-0.244}$
Durham, 0.05	8747.4	0.1512	9050.4	$-1.84^{+0.024}_{+0.013}$	9035.8	$-0.52^{+0.105}_{-0.147}$
Durham, 0.10	8747.4	0.1512	9018.2	$-1.46^{+0.019}_{+0.011}$	8992.4	$-0.38^{+0.076}_{-0.107}$
Durham, 0.15	8747.4	0.1512	8996.7	$-1.26^{+0.016}_{+0.009}$	8964.4	$-0.33^{+0.065}_{-0.091}$

Next we select two-jet events with the flavor- k_T and Durham algorithm and a specified resolution parameter y_{cut} . As in the inclusive case just discussed the axis of the b jet defines whether a jet lies in the forward or backward hemisphere. We calculate the resulting two-jet forward-backward asymmetry to NNLO QCD. The tree level-values A_{FB}^{LO} are of course the same as in table 12, and the NLO and NNLO QCD correction terms A_1^{2j} , A_2^{2j} are given in table 15. Comparing with the respective numbers in table 12 one sees that the QCD corrections to the two-jet asymmetry are significantly smaller than in the case of the

Table 13: The ratio A_2/A_1 for the two jet algorithms and the jet resolution parameters y_{cut} from table 12.

Flavor k_T, y_{cut}	0.01	0.05	0.10	0.15
A_2/A_1	37.9%	31.1%	28.1%	27.1%
Durham, y_{cut}	0.01	0.05	0.10	0.15
A_2/A_1	33.8%	28.5%	26.2%	26.0%

Table 14: The cross sections σ_S in units of pb at NNLO QCD at the Z peak for unpolarized beams and $\mu = m_Z$, with the forward and backward hemispheres defined with respect to the b -jet axis, without the contribution from the $b\bar{b}b\bar{b}$ final state and the resulting expansion terms A_2 of the FB asymmetry for two jet algorithms.

y_{cut}	Flavor k_T		Durham	
	σ_S [pb]	A_2	σ_S [pb]	A_2
0.01	9136.3	-0.0101	9101.4	-0.0082
0.05	9111.1	-0.0079	9027.9	-0.0051
0.10	9088.7	-0.0065	8985.1	-0.0037
0.15	9066.7	-0.0057	8957.3	-0.0032

inclusive b -jet A_{FB} . This makes the two-jet A_{FB} a candidate for a precision observable.

Table 15: The QCD correction terms A_1^{2j} , A_2^{2j} for the two-jet A_{FB} with respect to the b -jet axis using two jet algorithms with several y_{cut} . Here unpolarized e^+e^- beams are considered. The numbers for A_1^{2j} , A_2^{2j} and their scale variations are given in the unit of 10^{-2} .

y_{cut}	Flavor k_T			Durham		
	σ_S [pb]	A_1^{2j} [10^{-2}]	A_2^{2j} [10^{-2}]	σ_S [pb]	A_1^{2j} [10^{-2}]	A_2^{2j} [10^{-2}]
0.01	5781.3	$-0.151^{+0.002}_{-0.001}$	$0.029^{+0.017}_{-0.011}$	5984.9	$-0.168^{+0.002}_{-0.001}$	$0.032^{+0.018}_{-0.012}$
0.05	7666.2	$-0.390^{+0.005}_{-0.003}$	$-0.015^{+0.005}_{-0.002}$	8011.6	$-0.467^{+0.006}_{-0.003}$	$-0.090^{+0.012}_{-0.016}$
0.10	8231.5	$-0.571^{+0.007}_{-0.004}$	$-0.061^{+0.008}_{-0.010}$	8548.1	$0.696^{+0.009}_{-0.005}$	$-0.160^{+0.028}_{-0.038}$
0.15	8491.6	$-0.705^{+0.009}_{-0.005}$	$-0.109^{+0.018}_{-0.025}$	8754.7	$-0.851^{+0.011}_{-0.006}$	$-0.222^{+0.041}_{-0.057}$

The QCD correction to the two-jet A_{FB} becomes smaller in magnitude as y_{cut} becomes smaller,² which can be understood from the soft behavior of the amplitude. It follows from the fact that by enforcing more stringent two-jet cuts this asymmetry probes the soft

²This was observed before in [43] where the two-jet A_{FB} was computed to NNLO QCD for massless b quarks.

region, and the leading QCD soft contributions factorize and largely cancel in the two-jet A_{FB} . Actually, as the numbers in table 15 show, in the case of the flavor- k_T algorithm the magnitude of A_2^{2j} does not fall monotonously with decreasing y_{cut} . Yet, we checked that if only the flavor non-singlet contributions are taken into account $|A_2^{2j}|$ decreases with smaller y_{cut} , just as $|A_1^{2j}|$ does.

On the other hand, as already mentioned above, the QCD correction terms A_1 , A_2 for the inclusive b -jet FB asymmetry increase in magnitude, for both jet algorithms, as y_{cut} decreases, cf. the numbers in table 12. The NLO correction terms A_1 and A_2 approach, at very small y_{cut} , the corresponding values determined for the b -quark axis (cf. table 9). In particular, the sequence of numbers for the flavor- k_T algorithm shows this clearly, whereas in the case of the Durham jet algorithm A_1 changes significantly for $y_{cut} < 0.05$. This is understandable especially with the flavor- k_T algorithm, because for a tiny y_{cut} , the difference between the direction of the massive b -quark and that of the b -jet becomes very small for each event as the gluons within the jet are either soft or radiated almost collinear to the massive b -quark.

Moreover, by comparing tables 12 and 10, it is amusing to notice that the values of A_1 , A_2 of the thrust axis A_{FB} , which was used in the experimental measurements [61, 62], are very close to those of the inclusive b -jet A_{FB} in case of the flavor- k_T algorithm with $y_{cut} = 0.01$.

In principle, one may also determine the direction of the thrust axis using the momenta of the jets in eq. (4.1), rather than those of the partons, for each accepted event with at least one b -jet. The antisymmetric cross section determined in this way remains, to $\mathcal{O}(\alpha_s^2)$, the same as the one defined with the thrust axis determined by the parton momenta, while the symmetric b -jet cross section changes. This is because the events without b -jets (for instance those where a b -quark is combined with an anti- b -quark into a jet without b -flavor) will, by definition, not be included. On the other hand they do not contribute to the antisymmetric cross section. For instance, for the flavor- k_T algorithm and $y_{cut} = 0.1$, one obtains $A_1 = -0.0270$ and $A_2 = -0.0066$ when the thrust axis is determined by the momenta of the jets. These correction terms are smaller than the corresponding numbers in table 10.

We conclude the discussion of this section with a short comment on the effect of beam polarization on the b -jet forward-backward asymmetries. As far as the QCD corrections are concerned, beam polarization affects, as discussed above, only the NNLO terms A_2^{2j} and A_2 . In order to quantify the maximal spread of the NNLO correction terms we use again the ratio defined in eq. (3.2). In the flavor- k_T algorithm with jet resolution parameter $y_{cut} = 0.05$ and 0.1 , we get $|R_2^{\max}| = 12\%$ and 10% for $y_{cut} = 0.05$ and 0.1 , respectively, in case of the inclusive b -jet asymmetry. For the two-jet asymmetry we have $|R_2^{\max}| = 54\%$ and 17% . These numbers are deceptive, because in absolute terms, the NNLO QCD corrections A_2^{2j} are very small and significantly smaller than the QCD uncertainties due to the scale choice.

At this point we add, for completeness, a few remarks concerning the electroweak corrections to $b\bar{b}$ production and, in particular, to the b -quark asymmetries at the Z resonance. An overview of the order α QED corrections (real and virtual initial- and final-state

photonic corrections) and approximations to higher orders is given in [9] and references contained therein. Their size depends on the experimental set-up, i.e., on the photon cuts applied in an experiment. The most important corrections are the initial-state photonic corrections. A recent higher-order calculation in the logarithmic approximation was made in [63]; cf. also the references cited therein.

The purely weak corrections to the b -quark asymmetries are virtual corrections; i.e., affect all asymmetries by the same amount. They are model-dependent, that is, their size depends on whether they are computed in the Standard Model or some of its extension. The NLO weak SM corrections to the b -quark asymmetry have long been known, cf. [9] for an overview and references therein. They consist of vertex and box corrections and imaginary parts of propagator corrections. From the tables given in [9] one can infer, for the top quark mass of eq. (2.15), that the SM weak NLO corrections $\Delta A_{\text{FB}}^{\text{weak}}$ to the leading order b -quark asymmetry ($A_{\text{FB}} = A_{\text{FB}}^{\text{LO}} + \Delta A_{\text{FB}}^{\text{weak}} + \dots$) is of the order $\Delta A_{\text{FB}}^{\text{weak}} \simeq -0.0051$. The full two-loop vertex-type weak SM corrections and the mixed weak-QCD corrections were determined in [64–66]. The following remark is in order here. The experimental measurements of the b -quark asymmetries (the raw asymmetries) are not used directly in the electroweak fits. Instead, a so-called pseudo-observable is used by subtracting from the respective raw asymmetry some (almost) model independent corrections. These include QED corrections, γ – Z interference, and the QCD corrections [11, 61, 62, 67]. The pseudo-observable obtained in this way (that incorporates the weak corrections) is then used in a fit to obtain the effective weak mixing angle. Thus the QCD corrections to the b -quark asymmetries determined in this paper are an important ingredient in future analyses of this type.

Finally, we address the polarized b -quark forward-backward asymmetry (2.14). As we work to lowest order in the electroweak couplings and, therefore, take only Z -boson exchange at the Z peak into account, one expects that between $A_{\text{pol,FB}}$ and the corresponding asymmetry for unpolarized beams, A_{FB} , the following relation holds [51]:

$$A_{\text{FB}} = A_e A_{\text{pol,FB}} = \frac{2g_{Ve}g_{Ae}}{g_{Ve}^2 + g_{Ae}^2} A_{\text{pol,FB}}, \quad (4.4)$$

where g_{Ve} and g_{Ae} are the vector and axial-vector couplings of the electron to the Z boson. Using the value of $\sin^2 \theta_W$ listed in eq. (2.15) we get $A_{\text{FB}}/A_{\text{pol,FB}} = 0.2143$. We checked that this relation holds for the b -quark axis, thrust axis, and the b -jet axis definitions of the asymmetry with various y_{cut} ; i.e., it is not affected by the QCD corrections. On the other hand, in the case of top-quark pair production in the high energy limit $s \gg m_Z^2$, the leading order result for this ratio reads

$$\frac{A_{\text{FB}}}{A_{\text{pol,FB}}} = \frac{2g_{Ve}g_{Ae}g_{Vt} + g_{Ae}Q_eQ_t}{(g_{Ve}^2 + g_{Ae}^2)g_{Vt} + g_{Ve}Q_eQ_t}, \quad (4.5)$$

where g_{Vt} is the vector coupling of the top quark to the Z boson and Q_e and Q_t are the charges of the electron and top quark, respectively. Using the value of $\sin^2 \theta_W$ listed in eq. (2.15), we get $A_{\text{FB}}/A_{\text{pol,FB}} = 3.170$ which sets the high-energy limit for the numbers in table 8.

5 Conclusions

We have computed the second-order QCD corrections to the top-quark forward-backward asymmetry in $e^+e^- \rightarrow t\bar{t}$ collisions for various c.m. energies above the $t\bar{t}$ threshold and to several b -quark FB asymmetries at the Z resonance. These asymmetries should play an important role in precision studies, especially in the measurement of the electroweak couplings of heavy quarks at future electron-positron colliders. As a new feature we have investigated the effect of e^+ and e^- beam polarization. We have identified the contributions at NLO and NNLO QCD that are affected by polarized beams. We considered a set of benchmark polarizations and found that the relative effects of e^\pm polarizations on the QCD correction factors are, for $t\bar{t}$ production, quite sizeable. However, in absolute terms, they change the top-quark asymmetry only by an amount of the order of a few per mille, which is comparable to the projected uncertainty of this observable at future high-energy high-luminosity electron-positron colliders. In the case of $b\bar{b}$ production at the Z peak and to lowest order in the electroweak couplings only the NNLO QCD corrections are affected by beam polarization and the resulting overall effect on the b quark asymmetries is at the per mille level.

Our computational set-up allows also for the calculation of differential distributions, and we demonstrated this by determining the polar angle distribution of the top quark at $\sqrt{s} = 500$ GeV. We analyzed also, both for t and b quarks, the polarized forward-backward asymmetry that combines data taken with two opposite beam polarizations.

As to $b\bar{b}$ production at the Z peak we computed, apart for the FB asymmetries with respect to b -quark direction and the oriented thrust direction, also an inclusive b -jet asymmetry and a two-jet asymmetry, both for the flavor- k_T and the Durham jet clustering algorithm. The b -jet asymmetries were, to our knowledge, not yet investigated to NNLO QCD for massive b quarks. The QCD corrections to the two-jet asymmetry are significantly smaller than those of the other b -quark asymmetries. This qualifies it as a precision observable for the determination of the neutral-current couplings of b quarks.

Acknowledgments

This work was supported by the Natural Science Foundation of China under contract No.12205171, No.12235008.

References

- [1] A. Aryshev *et al.* [ILC International Development Team], “The International Linear Collider: Report to Snowmass 2021,” [arXiv:2203.07622 [physics.acc-ph]].
- [2] O. Brunner, P. N. Burrows, S. Calatroni, N. C. Lasheras, R. Corsini, G. D’Auria, S. Doeber, A. Faus-Golfe, A. Grudiev and A. Latina, *et al.* “The CLIC project,” [arXiv:2203.09186 [physics.acc-ph]].
- [3] S. Dasu, E. A. Nanni, M. E. Peskin, C. Vernieri, T. Barklow, K. Agashe, R. Bartoldus, P. C. Bhat, K. Black and J. Brau, *et al.* “Strategy for Understanding the Higgs Physics: The Cool Copper Collider,” [arXiv:2203.07646 [hep-ex]].
- [4] G. Bernardi, E. Brost, D. Denisov, G. Landsberg, M. Aleksa, D. d’Enterria, P. Janot, M. L. Mangano, M. Selvaggi and F. Zimmermann, *et al.* “The Future Circular Collider: a Summary for the US 2021 Snowmass Process,” [arXiv:2203.06520 [hep-ex]].
- [5] J. Gao [CEPC Accelerator Study Group], “Snowmass2021 White Paper AF3-CEPC,” [arXiv:2203.09451 [physics.acc-ph]].
- [6] A. Blondel and P. Janot, “Circular and Linear e^+e^- Colliders: Another Story of Complementarity,” [arXiv:1912.11871 [hep-ex]].
- [7] H. Cheng *et al.* [CEPC Physics Study Group], “The Physics potential of the CEPC. Prepared for the US Snowmass Community Planning Exercise (Snowmass 2021),” [arXiv:2205.08553 [hep-ph]].
- [8] W. Beenakker, S. C. van der Marck and W. Hollik, “ e^+e^- annihilation into heavy fermion pairs at high-energy colliders,” Nucl. Phys. B **365**, 24-78 (1991) doi:10.1016/0550-3213(91)90606-X.
- [9] M. Böhm, W. Hollik *et al.*, “Forward-Backward Asymmetries,” in: CERN Yellow Report, “Z Physics at LEP 1”, CERN 89-08 (1989), G. Altarelli *et al.* (eds.).
- [10] D. Y. Bardin, P. Christova, M. Jack, L. Kalinovskaya, A. Olchevski, S. Riemann and T. Riemann, “ZFITTER v.6.21: A Semianalytical program for fermion pair production in e^+e^- annihilation,” Comput. Phys. Commun. **133**, 229 (2001) [hep-ph/9908433].
- [11] A. Freitas and K. Mönig, “Corrections to quark asymmetries at LEP,” Eur. Phys. J. C **40**, 493 (2005) [hep-ph/0411304].
- [12] J. Fleischer, A. Leike, T. Riemann and A. Werthenbach, “Electroweak one loop corrections for e^+e^- annihilation into top anti-top including hard bremsstrahlung,” Eur. Phys. J. C **31**, 37-56 (2003) doi:10.1140/epjc/s2003-01263-8 [arXiv:hep-ph/0302259 [hep-ph]].
- [13] J. Jersak, E. Laermann and P. M. Zerwas, “Electroweak Production Of Heavy Quarks In e^+e^- Annihilation,” Phys. Rev. D **25**, 1218 (1982) [Erratum-ibid. D **36**, 310 (1987)].
- [14] A. B. Arbuzov, D. Y. Bardin, A. Leike, “Analytic final state corrections with cut for $e^+e^- \rightarrow$ massive fermions,” Mod. Phys. Lett. **A7**, 2029 (1992).
- [15] A. Djouadi, B. Lampe and P. M. Zerwas, “A Note on the QCD corrections to forward - backward asymmetries of heavy quark jets in Z decays,” Z. Phys. C **67**, 123-128 (1995) doi:10.1007/BF01564827 [arXiv:hep-ph/9411386 [hep-ph]].
- [16] T. Hahn, W. Hollik, A. Lorca, T. Riemann and A. Werthenbach, “ $\mathcal{O}(\alpha)$ electroweak corrections to the processes $e^+e^- \rightarrow \tau^-\tau^+, c\bar{c}, b\bar{b}, t\bar{t}$: A Comparison,” [arXiv:hep-ph/0307132 [hep-ph]].

- [17] P. H. Khien, J. Fujimoto, T. Ishikawa, T. Kaneko, K. Kato, Y. Kurihara, Y. Shimizu, T. Ueda, J. A. M. Vermaseren and Y. Yasui, “Full $\mathcal{O}(\alpha)$ electroweak radiative corrections to $e^+e^- \rightarrow t\bar{t}\gamma$ with GRACE-Loop,” *Eur. Phys. J. C* **73**, no.4, 2400 (2013) doi:10.1140/epjc/s10052-013-2400-3 [arXiv:1211.1112 [hep-ph]].
- [18] A. Arbuzov, S. Bondarenko and L. Kalinovskaya, “Asymmetries in Processes of Electron-Positron Annihilation,” *Symmetry* **12**, no.7, 1132 (2020) doi:10.3390/sym12071132 [arXiv:2007.03908 [hep-ph]].
- [19] S. G. Gorishnii, A. L. Kataev and S. A. Larin, “Three Loop Corrections of $\mathcal{O}(M^2)$ to the Correlator of Electromagnetic Quark Currents,” *Nuovo Cim. A* **92**, 119-131 (1986) doi:10.1007/BF02727185.
- [20] K. G. Chetyrkin, J. H. Kühn and M. Steinhauser, “Three loop polarization function of $\mathcal{O}(\alpha_s^2)$ corrections to the production of heavy quarks,” *Nucl. Phys. B* **482**, 213-240 (1996) doi:10.1016/S0550-3213(96)00534-2 [arXiv:hep-ph/9606230 [hep-ph]].
- [21] K. G. Chetyrkin, R. Harlander, J. H. Kühn and M. Steinhauser, “Mass corrections to the vector current correlator,” *Nucl. Phys. B* **503**, 339-353 (1997) doi:10.1016/S0550-3213(97)00383-0 [arXiv:hep-ph/9704222 [hep-ph]].
- [22] K. G. Chetyrkin, A. H. Hoang, J. H. Kühn, M. Steinhauser and T. Teubner, “Massive quark production in electron positron annihilation to order α_s^2 ,” *Eur. Phys. J. C* **2**, 137-150 (1998) doi:10.1007/s100520050128 [arXiv:hep-ph/9711327 [hep-ph]].
- [23] A. H. Hoang, V. Mateu and S. Mohammad Zabarjad, “Heavy Quark Vacuum Polarization Function at $\mathcal{O}(\alpha_s^2(s))$ and $\mathcal{O}(\alpha_s^3(s))$,” *Nucl. Phys. B* **813**, 349-369 (2009) doi:10.1016/j.nuclphysb.2008.12.005 [arXiv:0807.4173 [hep-ph]].
- [24] Y. Kiyo, A. Maier, P. Maierhofer and P. Marquard, “Reconstruction of heavy quark current correlators at $\mathcal{O}(\alpha_s^3)$,” *Nucl. Phys. B* **823**, 269-287 (2009) doi:10.1016/j.nuclphysb.2009.08.010 [arXiv:0907.2120 [hep-ph]].
- [25] I. Dubovyk, A. Freitas, J. Gluza, T. Riemann and J. Usovitsch, “Complete electroweak two-loop corrections to Z boson production and decay,” *Phys. Lett. B* **783**, 86-94 (2018) doi:10.1016/j.physletb.2018.06.037 [arXiv:1804.10236 [hep-ph]].
- [26] F. Bach, B. C. Nejad, A. Hoang, W. Kilian, J. Reuter, M. Stahlhofen, T. Teubner and C. Weiss, “Fully-differential Top-Pair Production at a Lepton Collider: From Threshold to Continuum,” *JHEP* **03**, 184 (2018) doi:10.1007/JHEP03(2018)184 [arXiv:1712.02220 [hep-ph]].
- [27] A. Denner, M. Pellen and G. Pelliccioli, “NLO QCD corrections to off-shell top-antitop production with semi-leptonic decays at lepton colliders,” [arXiv:2302.04188 [hep-ph]].
- [28] J. Gao and H. X. Zhu, “Top Quark Forward-Backward Asymmetry in e^+e^- Annihilation at Next-to-Next-to-Leading Order in QCD,” *Phys. Rev. Lett.* **113**, no.26, 262001 (2014) doi:10.1103/PhysRevLett.113.262001 [arXiv:1410.3165 [hep-ph]].
- [29] L. Chen, O. Dekkers, D. Heisler, W. Bernreuther and Z. G. Si, “Top-quark pair production at next-to-next-to-leading order QCD in electron positron collisions,” *JHEP* **12**, 098 (2016) doi:10.1007/JHEP12(2016)098 [arXiv:1610.07897 [hep-ph]].
- [30] M. Beneke, Y. Kiyo, P. Marquard, A. Penin, J. Piclum and M. Steinhauser, “Next-to-Next-to-Next-to-Leading Order QCD Prediction for the Top Antitop S -Wave Pair

- Production Cross Section Near Threshold in e^+e^- Annihilation,” *Phys. Rev. Lett.* **115**, no.19, 192001 (2015) doi:10.1103/PhysRevLett.115.192001 [arXiv:1506.06864 [hep-ph]].
- [31] M. Beneke, P. Marquard, P. Nason and M. Steinhauser, “On the ultimate uncertainty of the top quark pole mass,” *Phys. Lett. B* **775**, 63-70 (2017) doi:10.1016/j.physletb.2017.10.054 [arXiv:1605.03609 [hep-ph]].
 - [32] M. Beneke, Y. Kiyo, A. Maier and J. Piclum, “Near-threshold production of heavy quarks with `QQbar_threshold`,” *Comput. Phys. Commun.* **209**, 96-115 (2016) doi:10.1016/j.cpc.2016.07.026 [arXiv:1605.03010 [hep-ph]].
 - [33] M. Beneke, A. Maier, T. Rauh and P. Ruiz-Femenia, “Non-resonant and electroweak NNLO correction to the e^+e^- top anti-top threshold,” *JHEP* **02**, 125 (2018) doi:10.1007/JHEP02(2018)125 [arXiv:1711.10429 [hep-ph]].
 - [34] X. Chen, X. Guan, C. Q. He, X. Liu and Y. Q. Ma, “Heavy-quark-pair production at lepton colliders at NNNLO in QCD,” [arXiv:2209.14259 [hep-ph]].
 - [35] X. Liu, Y. Q. Ma and C. Y. Wang, “A Systematic and Efficient Method to Compute Multi-loop Master Integrals,” *Phys. Lett. B* **779**, 353-357 (2018) doi:10.1016/j.physletb.2018.02.026 [arXiv:1711.09572 [hep-ph]].
 - [36] X. Liu, Y. Q. Ma, W. Tao and P. Zhang, “Calculation of Feynman loop integration and phase-space integration via auxiliary mass flow,” *Chin. Phys. C* **45**, no.1, 013115 (2021) doi:10.1088/1674-1137/abc538 [arXiv:2009.07987 [hep-ph]].
 - [37] X. Liu and Y. Q. Ma, “Multiloop corrections for collider processes using auxiliary mass flow,” *Phys. Rev. D* **105**, no.5, 5 (2022) doi:10.1103/PhysRevD.105.L051503 [arXiv:2107.01864 [hep-ph]].
 - [38] Z. F. Liu and Y. Q. Ma, “Determining Feynman Integrals with Only Input from Linear Algebra,” *Phys. Rev. Lett.* **129**, no.22, 222001 (2022) doi:10.1103/PhysRevLett.129.222001 [arXiv:2201.11637 [hep-ph]].
 - [39] X. Liu and Y. Q. Ma, “AMFlow: A Mathematica package for Feynman integrals computation via auxiliary mass flow,” *Comput. Phys. Commun.* **283**, 108565 (2023) doi:10.1016/j.cpc.2022.108565 [arXiv:2201.11669 [hep-ph]].
 - [40] G. Altarelli and B. Lampe, “Second order QCD corrections to heavy quark forward - backward asymmetries,” *Nucl. Phys. B* **391**, 3-22 (1993) doi:10.1016/0550-3213(93)90138-F.
 - [41] V. Ravindran and W. L. van Neerven, “Second order QCD corrections to the forward - backward asymmetry in e^+e^- collisions,” *Phys. Lett. B* **445**, 214-222 (1998) doi:10.1016/S0370-2693(98)01436-1 [arXiv:hep-ph/9809411 [hep-ph]].
 - [42] S. Catani and M. H. Seymour, “Corrections of $O(\alpha_s^2)$ to the forward backward asymmetry,” *JHEP* **07**, 023 (1999) doi:10.1088/1126-6708/1999/07/023 [arXiv:hep-ph/9905424 [hep-ph]].
 - [43] S. Weinzierl, “The Forward-backward asymmetry at NNLO revisited,” *Phys. Lett. B* **644**, 331-335 (2007) doi:10.1016/j.physletb.2006.11.076 [arXiv:hep-ph/0609021 [hep-ph]].
 - [44] W. Bernreuther, L. Chen, O. Dekkers, T. Gehrmann and D. Heisler, “The forward-backward asymmetry for massive bottom quarks at the Z peak at next-to-next-to-leading order QCD,” *JHEP* **01**, 053 (2017) doi:10.1007/JHEP01(2017)053 [arXiv:1611.07942 [hep-ph]].
 - [45] S. Q. Wang, R. Q. Meng, X. G. Wu, L. Chen and J. M. Shen, “Revisiting the bottom quark forward-backward asymmetry A_{FB} in electron-positron collisions,” *Eur. Phys. J. C* **80**, no.7, 649 (2020) doi:10.1140/epjc/s10052-020-8234-x [arXiv:2003.13941 [hep-ph]].

- [46] S. J. Brodsky and X. G. Wu, “Eliminating the Renormalization Scale Ambiguity for Top-Pair Production Using the Principle of Maximum Conformality,” *Phys. Rev. Lett.* **109**, 042002 (2012) doi:10.1103/PhysRevLett.109.042002 [arXiv:1203.5312 [hep-ph]].
- [47] S. J. Brodsky and L. Di Giustino, “Setting the Renormalization Scale in QCD: The Principle of Maximum Conformality,” *Phys. Rev. D* **86**, 085026 (2012) doi:10.1103/PhysRevD.86.085026 [arXiv:1107.0338 [hep-ph]].
- [48] M. Mojaza, S. J. Brodsky and X. G. Wu, “Systematic All-Orders Method to Eliminate Renormalization-Scale and Scheme Ambiguities in Perturbative QCD,” *Phys. Rev. Lett.* **110**, 192001 (2013) doi:10.1103/PhysRevLett.110.192001 [arXiv:1212.0049 [hep-ph]].
- [49] S. Catani, Y. L. Dokshitzer, M. Olsson, G. Turnock and B. R. Webber, “New clustering algorithm for multi-jet cross-sections in e^+e^- annihilation,” *Phys. Lett. B* **269**, 432-438 (1991). doi:10.1016/0370-2693(91)90196-W.
- [50] A. Banfi, G. P. Salam and G. Zanderighi, “Infrared safe definition of jet flavor,” *Eur. Phys. J. C* **47**, 113-124 (2006) doi:10.1140/epjc/s2006-02552-4 [arXiv:hep-ph/0601139 [hep-ph]].
- [51] A. Blondel, B. W. Lynn, F. M. Renard and C. Verzegnassi, “Precision Measurements of Final State Weak Coupling From Polarized Electron - Positron Annihilation,” *Nucl. Phys. B* **304**, 438-450 (1988) doi:10.1016/0550-3213(88)90636-0.
- [52] R. L. Workman et al. [Particle Data Group], “Review of Particle Physics,” *Prog. Theor. Exp. Phys.* **2022**, 083C01 (2022) doi:10.1093/ptep/ptac097.
- [53] W. Bernreuther, C. Bogner and O. Dekkers, “The real radiation antenna functions for $S \rightarrow Q\bar{Q}gg$ at NNLO QCD,” *JHEP* **10**, 161 (2013) doi:10.1007/JHEP10(2013)161 [arXiv:1309.6887 [hep-ph]].
- [54] W. Bernreuther, C. Bogner and O. Dekkers, “The real radiation antenna function for $S \rightarrow Q\bar{Q}q\bar{q}$ at NNLO QCD,” *JHEP* **06**, 032 (2011) doi:10.1007/JHEP06(2011)032 [arXiv:1105.0530 [hep-ph]].
- [55] O. Dekkers and W. Bernreuther, “The real-virtual antenna functions for $S \rightarrow Q\bar{Q}X$ at NNLO QCD,” *Phys. Lett. B* **738**, 325-333 (2014) doi:10.1016/j.physletb.2014.09.060 [arXiv:1409.3124 [hep-ph]].
- [56] H. Abramowicz *et al.* [ILD Concept Group], [arXiv:2003.01116 [physics.ins-det]].
- [57] H. Abramowicz *et al.* [CLICdp], *JHEP* **11**, 003 (2019) doi:10.1007/JHEP11(2019)003 [arXiv:1807.02441 [hep-ex]].
- [58] E. Farhi, “A QCD Test for Jets,” *Phys. Rev. Lett.* **39**, 1587-1588 (1977) doi:10.1103/PhysRevLett.39.1587.
- [59] S. Brandt, C. Peyrou, R. Sosnowski and A. Wroblewski, “The Principal axis of jets. An Attempt to analyze high-energy collisions as two-body processes,” *Phys. Lett.* **12**, 57-61 (1964) doi:10.1016/0031-9163(64)91176-X.
- [60] S. Brandt and H. D. Dahmen, “Axes and Scalar Measures of Two-Jet and Three-Jet Events,” *Z. Phys. C* **1**, 61 (1979) doi:10.1007/BF01450381.
- [61] S. Schael *et al.* [ALEPH, DELPHI, L3, OPAL, SLD, LEP Electroweak Working Group, SLD Electroweak Group and SLD Heavy Flavour Group], “Precision electroweak measurements on the Z resonance,” *Phys. Rept.* **427**, 257-454 (2006) doi:10.1016/j.physrep.2005.12.006 [arXiv:hep-ex/0509008 [hep-ex]].

- [62] [ALEPH, CDF, D0, DELPHI, L3, OPAL, SLD, LEP Electroweak Working Group, Tevatron Electroweak Working Group, SLD Electroweak and Heavy Flavour Groups], “Precision Electroweak Measurements and Constraints on the Standard Model,” [arXiv:1012.2367 [hep-ex]].
- [63] J. Blümlein, A. De Freitas and K. Schönwald, “The QED initial state corrections to the forward-backward asymmetry of $e^+e^- \rightarrow \gamma^*/Z^{0*}$ to higher orders,” Phys. Lett. B **816**, 136250 (2021) doi:10.1016/j.physletb.2021.136250 [arXiv:2102.12237 [hep-ph]].
- [64] M. Awramik, M. Czakon, A. Freitas and G. Weiglein, “Complete two-loop electroweak fermionic corrections to $\sin^2 \theta_{\text{eff}}^{\text{lept}}$ and indirect determination of the Higgs boson mass,” Phys. Rev. Lett. **93**, 201805 (2004) doi:10.1103/PhysRevLett.93.201805 [arXiv:hep-ph/0407317 [hep-ph]].
- [65] M. Awramik, M. Czakon and A. Freitas, “Electroweak two-loop corrections to the effective weak mixing angle,” JHEP **11**, 048 (2006) doi:10.1088/1126-6708/2006/11/048 [arXiv:hep-ph/0608099 [hep-ph]].
- [66] M. Awramik, M. Czakon, A. Freitas and B. A. Kniehl, “Two-loop electroweak fermionic corrections to $\sin^2 \theta_{\text{eff}}^{b\bar{b}}$,” Nucl. Phys. B **813**, 174-187 (2009) doi:10.1016/j.nuclphysb.2008.12.031 [arXiv:0811.1364 [hep-ph]].
- [67] D. Abbaneo *et al.* [LEP Heavy Flavor Working Group], “QCD corrections to the forward-backward asymmetries of c and b quarks at the Z pole,” Eur. Phys. J. C **4** (1998) 185.